Fiber orientation estimation by constrained spherical deconvolution of the anisotropic edge illumination X-ray dark field signal

Ben Huyge[a,b], Ben Jeurissen[a], Jan De Beenhouwer[a,b], and Jan Sijbers[a,b]

[a]imec-Vision Lab, Departement of Physics, University of Antwerp, Belgium
[b]DynXlab: Center for 4D Quantitative X-ray Imaging and Analysis, Antwerp, Belgium

ABSTRACT

Determining fiber orientations in a fiber reinforced material with X-ray CT is challenging because the width of the individual fibers is often much smaller than the spatial resolution of the X-ray images. However, the anisotropic X-ray scattering signal of the fibers yields information about the fiber direction without the need to individually resolve them. In this work, edge illumination phase contrast imaging is used to sample the anisotropic X-ray scattering in the object along different directions. The measured scatter is represented on a sphere by a set of spherical harmonics. Next, the orientation of the fibers is extracted from the scatter function by constrained spherical deconvolution. This approach is experimentally validated, for both parallel and crossing fiber distributions in a single voxel, using Monte Carlo simulations in GATE. The retrieved fiber orientations for parallel and crossing carbon fibers are presented as result.

Keywords: X-ray phase contrast imaging, anisotropic dark field, fibers, edge illumination, spherical deconvolution

1. INTRODUCTION

Carbon fiber reinforced polymers (CFRP) have useful material properties like high stiffness, while being relatively lightweight compared to for example steel. This makes them attractive for use in aerospace and automotive industry or in manufacturing processes.[1] The properties of these fiber reinforced materials depend strongly on the fiber orientation distribution (FOD) within the material,[2] so gaining information about the FOD is vital for quality inspection.

X-ray computed tomography (XCT) is a key imaging technique to nondestructively visualize the FOD. However, the fibers typically have a diameter in the micrometer range so to resolve them, an expensive high resolution detector is necessary.[3] Moreover, conventional XCT is solely sensitive to attenuation contrast. Since fibers and the resin in CFRP exhibit similar X-ray attenuation, distinguishing them based on attenuation contrast alone can be challenging.[4]

Edge illumination X-ray phase contrast imaging (EI-XPCI) provides additional value through its sensitivity to multiple complementary contrasts. It is a noninterferometric XPCI-technique that, besides conventional attenuation contrast, is also sensitive to X-ray refraction and X-ray scattering, denoted as the phase contrast and dark field contrast, respectively.[5] The dark field contrast is especially suited to visualize the FOD because of how the contrast is generated. It arises from X-ray scattering caused by repeated refractions at microstructures in the material. When these microstructures have a characteristic direction (e.g., fibers) the X-ray scattering is anisotropic, which provides information about the orientation of the fibers.[6] A major advantage of dark field contrast imaging is that the scatter information can be measured without needing to individually resolve the fibers, eliminating the need for a detector with super-high resolution that often limits the field of view.

Wieczoreck et al.[7,8] uses grating interferometry to measure the anisotropic dark field signal. Spherical harmonics are then used to represent the scatter function from which the FOD is extracted. However, to our knowledge the extraction of the FOD is not yet validated using EI-XPCI.

Further author information:
B. Huyge: E-mail: ben.huyge@uantwerpen.be

In this paper, the approach of Wieczoreck is implemented for an EI-XPCI setup and expanded by adding constrained spherical deconvolution as a transformation from the measured scattering function to the FOD. The results are obtained using computer simulations in GATE, a Monte Carlo based simulation framework for tomographic imaging.[9]

2. METHODS

2.1 Edge illumination

In EI-XPCI, two masks are added to the conventional XCT setup: a sample mask and a detector mask. These masks consist of slit-shaped apertures alternating with a highly absorbing material (e.g., gold). The sample mask splits the incoming X-ray beam into separate smaller beams. The detector mask is positioned right in front of the detector so that the apertures are aligned with the center of each detector pixel, thereby covering the pixel edges. In an EI-XPCI scan, the sample mask is stepped so the beamlets shift over the uncovered part of the pixels. For each pixel a Gaussian function is fitted to the measured intensity in function of the sample mask displacement, denoted as the illumination curve (IC). When an object is introduced in the setup and the stepping of the mask is repeated, the IC changes. X-ray attenuation lowers the surface area underneath the IC, while X-ray refraction shifts the position of maximum intensity. The dark field contrast relates to the X-ray scattering and results in a broadening of the IC. A complete explanation of EI-XPCI is given in Ref. 5.

2.2 Anisotropic dark field tomography

In the work of Wieczoreck on anisotropic dark field tomography the dark field signal is reconstructed as a function η on the unit sphere $\mathbb{S}_2$ using spherical harmonics.[7] In their work, the dark field signal is described as follows:

$$d_j = \exp\left(-\int_{L_j}\int_{\mathbb{S}_2} h(\mathbf{u},\mathbf{t}_j,\mathbf{l}_j)\eta(\mathbf{u},x)\frac{d\Omega(\mathbf{u})}{4\pi}dx\right), \tag{1}$$

where d_j is the j^{th} dark field measurement, L_j is the line of the X-ray beam and Ω denotes the solid angle. The weight function $h(\mathbf{u},\mathbf{t}_j,\mathbf{l}_j)$ depends on the direction on the unit sphere $\mathbf{u}\in\mathbb{S}_2$, as well as on the beam direction $\mathbf{l}_j\in\mathbb{S}_2$ and the sensitivity direction $\mathbf{t}_j\in\mathbb{S}_2$ of the setup, which is orthogonal to the aperture slits direction. The weight function is defined as

$$h(\mathbf{u},\mathbf{t}_j,\mathbf{l}_j) = \left(|\mathbf{l}_j\times\mathbf{u}|(\mathbf{t}_j\cdot\mathbf{u})\right)^2, \tag{2}$$

with '$\times$' denoting the vector product, '$\cdot$' the scalar product and '$|...|$' the Euclidean norm.[10]

The model as described in Eq. (1) is specifically developed for grating interferometry, a different phase contrast imaging technique where the dark field signal is measured through the visibility, which decays exponentially with increasing scattering width.[11] However, in EI-XPCI, the measured dark field signal (broadening of the IC) increases with increasing scattering. Therefore, a first adaptation to the existing model comprises of removing the exponential function, yielding

$$d_j = \int_{L_j}\int_{\mathbb{S}_2} h(\mathbf{u},\mathbf{t}_j,\mathbf{l}_j)\eta(\mathbf{u},x)\frac{d\Omega(\mathbf{u})}{4\pi}dx. \tag{3}$$

In Ref. 7, the model is further discretized by expanding h and η into a series of spherical harmonics and using their orthonormal properties:

$$d_j \approx \frac{1}{4\pi}\sum_{k=0}^{K}\sum_{m=-k}^{k} h_k^m(\mathbf{t}_j,\mathbf{l}_j)\int_{L_j}\eta_k^m(x)dx. \tag{4}$$

Here, h_k^m and η_k^m are the coefficients of real valued spherical harmonics of degree k and order m, representing the weight and scatter function. Then Eq. (4) is written as a system of linear equations by dividing the reconstruction volume into I voxels and discretizing the line integral, resulting in

$$\mathbf{d} = \sum_{k=0}^{K}\sum_{m=-k}^{k}\mathbf{W}_k^m\mathbf{P}\boldsymbol{\eta}_k^m, \tag{5}$$

where $\mathbf{d} \in \mathbb{R}^J$ is the vector with the J measurements, $\mathbf{W}_k^m \in \mathbb{R}^{J\times J}$ is a diagonal matrix with the coefficients of the weight function $h_k^m(\mathbf{t}_j, \mathbf{l}_j)/4\pi$ on the diagonal and $\mathbf{P} \in \mathbb{R}^{J\times I}$ is the tomographic system matrix. This system is solved for the vector of unknown coefficients of the scatter function $\boldsymbol{\eta}_k^m \in \mathbb{R}^I$.[7]

2.3 Constrained spherical deconvolution with MRtrix3

In Ref. 8, the fiber orientation is extracted from the scatter function η with a Funk-Radon transform, where it is assumed that the measured scattering is higher when the scattering direction is orthogonal to the fibers. This assumption is avoided by using spherical deconvolution of the scatter function in a similar way as is done in diffusion weighted MRI. In this technique, the measured data $S(\theta, \phi)$ is described as a spherical convolution between a response function $R(\theta)$ and the FOD $F(\theta, \phi)$,

$$S(\theta, \phi) = F(\theta, \phi) \otimes R(\theta), \tag{6}$$

where θ and ϕ denote the spherical coordinates on the unit sphere.[12] In EI-XPCI, the function $S(\theta, \phi)$ represents the retrieved scatter function η, obtained from Eq. (5). The FOD is extracted by deconvolving S with the response function R, obtained from measuring the scatter function of a population of parallel fibers. Spherical deconvolution is an ill-conditioned problem, so constraints are added to avoid negative amplitudes in the FOD.[13] The constrained spherical deconvolution is performed with MRtrix3, a software framework for analyzing MRI data.[14]

2.4 Simulations in GATE

Our approach was experimentally validated using GATE simulations,[9] augmented with additional tools to introduce phase effects.[15] The simulation was modelled after the UnitomXL FleXCT Tescan scanner available at imec-Vision Lab.[16] The detector had a pixel width of 150 µm and was positioned at a distance of 1800 mm from the source (monochromatic, 25 keV) with a square focal spot of 20 µm. The detector mask had an aperture width of 30 µm and a period of 148 µm. To match the period of the detector mask with the period of the pixels, the mask was placed 24 mm in front of the detector. The sample mask had an aperture width of 20 µm, a period of 100 µm and was placed 600 mm before the detector. Both masks had a thickness of 225 µm and were made of perfectly absorbing material. During the scan the sample mask was shifted to five different positions [−18 µm, −9 µm, 0 µm, 9 µm, 18 µm], where 0 µm corresponds to the center position with maximal illumination.

The sample was introduced at a distance of 599.5 mm from the detector, right behind the sample mask. The sample was modelled as a box with a side of 0.1 mm that fits in one voxel. Inside the box, 1500 carbon fibers were placed with a length of 40 µm and a radius of 2 µm. To adequately sample the scatter in different directions around the object, the acquisition scheme of Sharma et al.[17] was used, where a set of sensitivity directions is uniformly distributed over the unit sphere. Each sensitivity direction is fully sampled by a subset of equally spaced beam directions on a circular trajectory in the plane orthogonal to the sensitivity direction. Here, 50 sensitivity directions were chosen, each sampled with 100 beam directions yielding 5000 sampling points in total.

3. RESULTS & DISCUSSION

By solving Eq. (5) with CGLS and a maximum degree $K = 4$, the scatter functions are obtained for different fiber distributions. In Fig. 1a) and 1b), scatter functions are shown for a distribution of parallel oriented fibers in the z-direction and the [111]-diagonal direction, respectively. Here, the scatter function is a disk with some axial symmetry around the fiber direction. Fig. 1c) shows the scatter function from a distribution of crossing fibers, where half of the fibers point in the z-direction and the other half in the x-direction. In Fig. 1d) the fiber populations make an angle of 70° instead of 90°.

The scatter functions in Fig. 1 are deconvolved in MRtrix3 with the scatter function in Fig. 1a) acting as response function, yielding the FODs shown in Fig. 2. The FODs show the direction of the fiber bundles, making it easier to interpret in comparison to the scatter functions. It is clearly shown that the directions are correctly extracted with the constrained spherical deconvolution. However, if two fiber populations cross at smaller angles (< 45°), the method may not be able to distinguish the two separate populations. This is subject to further research.

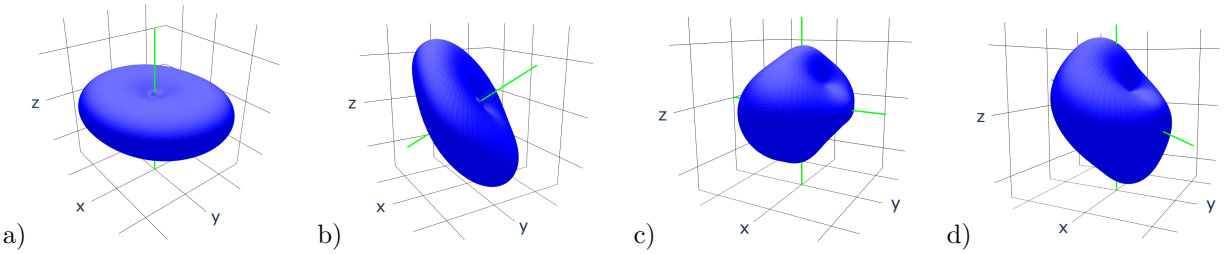

Figure 1. The scatter functions for different fiber distributions. The green line indicates the direction of the fiber.

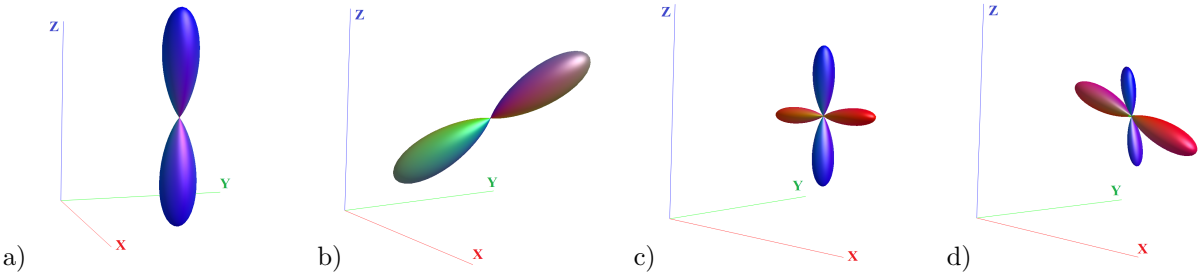

Figure 2. The FODs belonging to the scatter functions in Fig. 1. The color of the function is linked to the orientation indicated by the axes.

4. CONCLUSION

In this work, the method of Wieczoreck et al.[7] for anisotropic dark field tomography was implemented with EI-XPCI. The scatter functions of both parallel and crossing fiber distributions in a voxel were successfully retrieved. Additionally, a constrained spherical deconvolution step was used to transform the scatter function to the FOD, which displays the orientation of the fiber distributions. These techniques were validated based on simulations in GATE.

ACKNOWLEDGMENTS

This research was supported by the FWO (Research Foundation - Flanders) (1S46122N)

REFERENCES

[1] Carter, H., "Lighter, stiffer, faster – The case for carbon fiber composites in machinery," *Reinf. Plast* **64**, 57–59 (2020).

[2] Subhedar, K. M., Chauhan, G. S., Singh, B. P., and Dhakate, S. R., "Effect of fibre orientation on mechanical properties of carbon fibre composites," *IJEMS* **27**, 1100–1103 (2020).

[3] Cai, G., Shirai, T., Wan, Y., Uzawa, K., and Takahashi, J., "Application of X-ray computed tomography to measuring fiber orientation distribution of chopped carbon fiber tape reinforced thermoplastics," *Appl. Compos. Mater.* **28**, 573–586 (2021).

[4] Gresil, M. et al., "EVITA Project: Comparison between traditional non-destructive techniques and phase contrast X-ray imaging applied to aerospace carbon fibre reinforced polymer," *Appl. Compos. Mater.* **24**, 513–524 (2017).

[5] Olivo, A., "Edge-illumination x-ray phase-contrast imaging," *J. Phys.: Condens. Matter* **33**, 363002 (2021).

[6] Graetz, J., Balles, A., Hanke, R., and Zabler, S., "Review and experimental verification of x-ray dark-field signal interpretations with respect to quantitative isotropic and anisotropic dark-field computed tomography," *Phys. Med. Biol.* **65**, 235017 (2020).

[7] Wieczoreck, M., Schaff, F., Pfeiffer, F., and Lasser, T., "Anisotropic X-ray dark-field tomography: A continuous model and its discretization," *Phys. Rev. Lett.* **117**, 158101 (2016).

[8] Wieczoreck, M., Schaff, F., Jud, C., Pfeiffer, D., Pfeiffer, F., and Lasser, T., "Brain connectivity exposed by anisotropic X-ray dark-field tomography," *Sci. Rep* **8**, 14345 (2018).

[9] Jan, S. et al., "GATE: a simulation toolkit for PET and SPECT," *Phys. Med. Biol.* **49**, 4543–4561 (2004).

[10] Malecki, A. et al., "X-ray tensor tomography," *EPL* **105**, 38002 (2014).

[11] Bech, M., Bunk, O., Donath, T., Feidenhans'l, R., David, C., and Pfeiffer, F., "Quantitative x-ray dark-field computed tomography," *Phys. Med. Biol.* **55**, 5529–5539 (2010).

[12] Tournier, J.-D., Calamante, F., Gadian, D. G., and Connelly, A., "Direct estimation of the fiber orientation density function from diffusion-weighted MRI data using spherical deconvolution," *NeuroImage* **23**, 1176–1185 (2004).

[13] Tournier, J.-D., Calamante, F., and Connelly, A., "Robust determination of the fibre orientation distribution in diffusion MRI: Non-negativity constrained super-resolved spherical deconvolution," *NeuroImage* **35**, 1459–1472 (2007).

[14] Tournier, J.-D. et al., "MRtrix3: A fast, flexible and open software framework for medical image processing and visualisation," *NeuroImage* **202**, 116137 (2019).

[15] Sanctorum, J., De Beenhouwer, J., and Sijbers, J., "X-ray phase contrast simulation for grating-based interferometry using GATE," *Opt. Express* **28**, 33390–33412 (2020).

[16] De Samber, B. et al., "FleXCT: a flexible X-ray CT scanner with 10 degrees of freedom," *Opt. Express* **29**, 3438–3457 (2021).

[17] Sharma, M., Schaff, F., Wieczoreck, M., Pfeiffer, F., and Lasser, T., "Design of acquisition schemes and setup geometry for anisotropic X-ray dark-field tomography (AXDT)," *Sci. Rep.* **7**, 3195 (2017).